

# Bokeelamides: Lipopeptides from Bacteria Associated with Marine Egg Masses

Rose Campbell, Lois Kyei, Karla Piedl, Zheye Zhang, Ming Chen, and Emily Mevers\*



Cite This: *Org. Lett.* 2024, 26, 9693–9697



Read Online

ACCESS |



Metrics & More

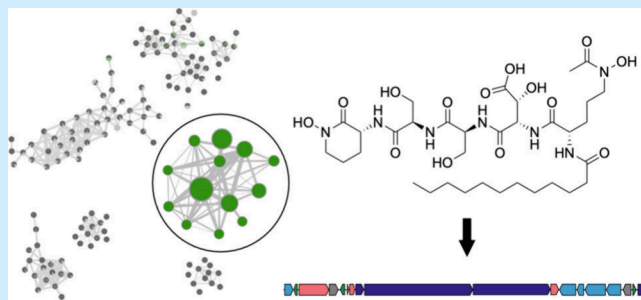


Article Recommendations



Supporting Information

**ABSTRACT:** Moon snails (family: Naticidae) lay egg masses that are rich in bacterial species distinct from the surrounding environment. We hypothesized that this microbiome chemically defends the moon snail eggs from predation and pathogens. Herein, we report the discovery of bokeelamides, new lipopeptides from the egg mass-associated bacterium, *Ectopseudomonas khazarica*, which were discovered using mass spectrometry (MS)-based metabolomics. The structures of the bokeelamides were elucidated using two-dimensional (2D) nuclear magnetic resonance (NMR), tandem MS, Marfey's, and genomic analyses.



Natural products are commonly deployed as defensive agents and have fascinated chemists for generations due to their structural complexity and pharmaceutical potential.<sup>1–5</sup> Many animals are known to form symbiotic relationships with chemically rich microorganisms, where the host provides essential nutrients in exchange for defensive agents.<sup>4,6–8</sup> Recently, our group showed that egg masses laid by *Neverita delessertiana*, a carnivorous moon snail, contain a chemically rich core bacterial microbiome that is distinct from the surrounding environment.<sup>9</sup> We hypothesize that this microbiome produces natural products to protect the egg masses from biofouling and predation.<sup>10</sup> Herein, we used a metabolomic approach to identify a new family of lipopeptides, bokeelamides.

As part of our continued effort to probe the natural product potential of moon snail egg mass-associated bacteria, we reanalyzed high-resolution tandem mass spectrometry (HR-MS/MS) data acquired on semicrude fractions representing 66 distinct bacterial strains using Global Natural Product Social (GNPS) molecular networking (Figure S1 of the Supporting Information). One subnetwork contained 13 nodes with precursor masses ranging from 762 to 846 Da (Figure 1) with no known library matches within the subnetwork. Traditional dereplication efforts, searching the molecular formula and/or the parent mass in AntiBase,<sup>11</sup> NPAtlas,<sup>12</sup> SIRIUS,<sup>13</sup> and SciFinder, failed to yield any hits to known chemistry. Although dereplication by SIRIUS yielded no exact matches, SIRIUS uses patterns in the tandem mass spectral data to derive structural information, and this analysis did suggest that these metabolites are peptidic. The SIRIUS analysis revealed the presence of distinguishable neutral losses corresponding to two serine residues (Figures S2–S4 of the Supporting Information).<sup>13</sup> Many of the nodes within the subnetwork differ from one another by 2 or 14 Da, suggesting

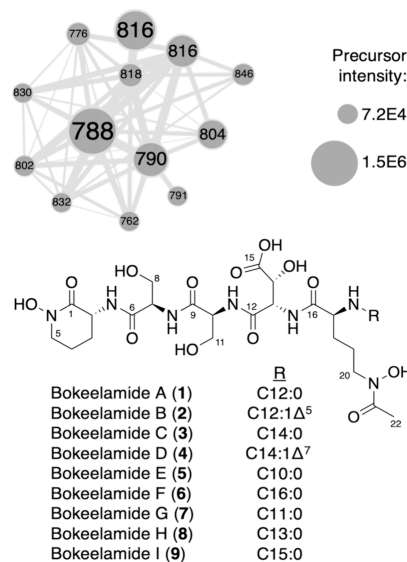


**Figure 1.** Subnetwork containing precursor masses (node labels) for bokeelamides.

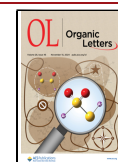
that the structural modification involved a change in either the degree of unsaturation (DoU) or methylene incorporation, respectively. The nodes are produced by five bacterial strains in our library, including two *Ectopseudomonas* strains (EM133

**Received:** September 16, 2024

**Revised:** October 28, 2024

**Accepted:** October 31, 2024

**Published:** November 1, 2024



and EM143), a *Bacillus* sp. (EM91), a *Pseudoalteromonas* sp. (EM135), and a *Vibrio* sp. (EM103). Only EM133, *Ectopseudomonas khazarica*, produces all 13 masses (Table S1 of the Supporting Information). Reverse-phase high-performance liquid chromatography led to the purification of the four major compounds (Figure S5 of the Supporting Information), named bokeelamides A–D (1–4).

We began our structure elucidation efforts by analyzing two-dimensional (2D) nuclear magnetic resonance (NMR) [ $^1\text{H}$ ,  $^{13}\text{C}$ , gradient-selected heteronuclear single quantum coherence (gHSQC), double-quantum-filtered correlation spectroscopy (dqfCOSY), total correlation spectroscopy (TOCSY), heteronuclear two-bond correlation (H2BC), and heteronuclear multiple-bond correlation (HMBC)] spectra of compound 1 as it was the most abundant and appeared to be the least complicated. Analysis of the high-resolution mass spectrometry (HRMS) data indicated that compound 1 had a molecular formula (MF) of  $\text{C}_{34}\text{H}_{59}\text{N}_7\text{O}_{14}$ . Partial structures were assembled using key 2D NMR correlations, revealing the presence of two modified ornithines (Orn), two serines (Ser), a  $\beta$ -hydroxy aspartic acid ( $\beta\text{OH-Asp}$ ), and a saturated lipid (C12:0) (Figures S6–S12 and Table S2 of the Supporting Information). A key HMBC between H-5 ( $\delta_{\text{H}}$  3.46) and C-1 ( $\delta_{\text{C}}$  165.0) indicated that the terminal Orn<sub>1</sub> residue has been cyclized. Reanalysis of the heteronuclear single-quantum correlation (HSQC) spectrum confirmed the presence of eight exchangeable protons, five of which ( $\delta_{\text{H}}$  7.76, 7.80, 8.07, 8.26, and 8.27) are part of the peptide backbone. HMBCs between these exchangeable protons and the neighboring amino acids established connectivity between the individual residues (Figure 2A). However,  $\text{C}_2\text{H}_5\text{O}_3$  was still left unassigned, and this included an obvious singlet methyl, C-22 ( $\delta_{\text{H}}$  1.99;  $\delta_{\text{C}}$  20.4). Analysis of the HMBCs from H<sub>3</sub>-22 showed a correlation to an unassigned carbonyl, C-21 ( $\delta_{\text{C}}$

170.4), matching the expected chemical shifts for an acetate moiety. In addition, an exchangeable proton at  $\delta_{\text{H}}$  5.31 had a TOCSY correlation to H<sub>3</sub>-22; however, there were no correlations between these protons and the established peptide core. Therefore, we used tandem mass spectrometry (MS/MS) to locate the positions of the remaining unassigned acetate moiety and hydroxyl groups. A key  $b_1$  fragment at  $m/z$  355.2584 represents Orn<sub>2</sub>-C12:0 but contains an additional  $\text{C}_2\text{H}_4\text{O}_2$ , suggesting that Orn<sub>2</sub> is both acetylated and hydroxylated (Figure 2B). Another key fragment,  $y_1$ , was  $m/z$  131.0813 indicating that cyclic Orn<sub>1</sub> is also hydroxylated, forming  $\text{N}^5\text{OH-Orn}_1$  and establishing the final planar structure of compound 1 as (cyclic- $\text{N}^5\text{OH-Orn}_1$ )-Ser<sub>1</sub>-Ser<sub>2</sub>-( $\beta\text{OH-Asp}$ )-(AcN<sup>5</sup>OH-Orn<sub>2</sub>)-C12:0.

The MFs and fragmentation patterns of compounds 2–4 are highly similar to those of compound 1. All  $y$  fragments were present in compounds 1–4, but the  $b$  fragments, representing lipid-containing portions, were shifted by the observed difference in the precursor mass (Figure 2B). Thus, the modifications within these analogues are restricted to the  $b_1$  fragment (Orn<sub>2</sub> and the lipid). As AcN<sup>5</sup>OH-Orn<sub>2</sub>-lipid did not fragment independently, we used NMR experiments to identify the structural modifications. Compound 2 is 2 Da less than compound 1, which corresponds to an increase in DoU. The HSQC spectrum revealed the presence of two  $\text{sp}^2$ -hybridized carbons that are part of an olefin ( $\delta_{\text{H}}$  5.30 and 5.33;  $\delta_{\text{C}}$  129.1 and 130.2). H2BCs confirmed that compound 2 incorporated a C12:1 $\Delta^5$  lipid (Figures S13–S19 and Table S3 of the Supporting Information). By HRMS, compounds 3 and 4 both incorporate an additional  $\text{C}_2\text{H}_4$  unit (28 Da) compared to compounds 1 and 2, respectively, which was hypothesized to represent an extension of the lipid. The NMR data for compound 3 was similar to those for compound 1, with the exception that the  $\text{CH}_2$  envelope integrated to 18 versus 16. Similarly, the NMR data for compound 4 was similar to those for compound 2, but analysis of H2BC spectra confirmed that compound 4 incorporates a C14:1 $\Delta^7$  lipid rather than a C12:1 $\Delta^5$  lipid (Figures S20–S31 and Tables S4 and S5 of the Supporting Information). To determine the stereoconfiguration of the olefin in compounds 2 and 4, we compared the experimental  $^{13}\text{C}$  shifts of the allylic methylenes to predicted chemical shifts of the *trans/cis* analogues using ChemDraw. All allylic methylenes were between 26.3 and 26.7 ppm, which matched closely to the *cis* configuration (26.7–27.7 ppm) over the *trans* configuration (32.7–33.7 ppm).

The GNPS cluster containing compounds 1–4 consisted of 13 nodes, with 7 nodes representing minor analogues with isolated yields too low for 2D NMR analysis. All nodes contained the same  $y_{1-4}$  ions, indicating that the modifications of the minor analogues were confined to either Orn<sub>2</sub> or the lipid. The MFs of compounds 5 and 6 indicated a loss of two methylenes from compound 1 and a gain in two methylenes from compound 3, suggesting incorporation of C10:0 and C16:0 lipids, respectively. The MFs for compounds 7–9 differ from compounds 5, 1, and 3, respectively, by the addition of one methylene, which was located using pseudo-MS<sup>3</sup> experiments, where the deacetylated  $b_1$  ion (OH-Orn<sub>2</sub>-lipid fragment) observed in the precursor spectrum was selected for further fragmentation. This generated fragments at  $m/z$  131 ( $\text{N}^5\text{OH-Orn}_2$ ), 114 (deaminated  $\text{N}^5\text{OH-Orn}_2$ ), or 113 ( $\text{Orn}_2$ ) (Figures S32–S34 of the Supporting Information) indicating that all modifications were restricted to the lipids, which were now identified as C11:0 (7), C13:0 (8), and C15:0 (9). The

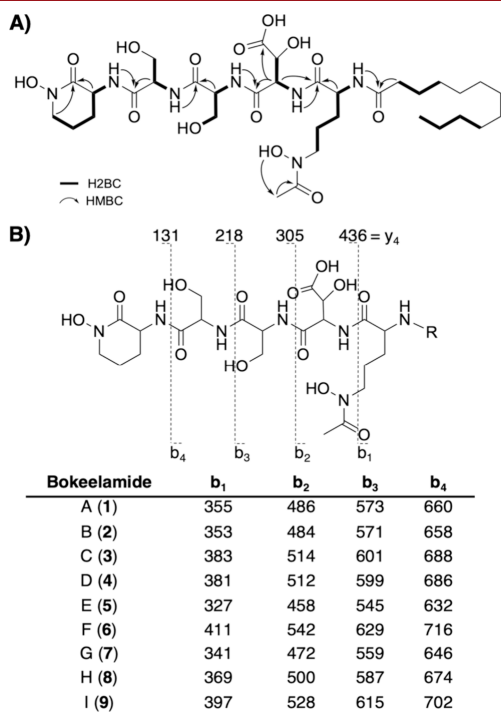


**Figure 2.** (A) Key 2D NMR correlations for bokeelamide A (1) and (B) observed fragmentation of bokeelamides, where all analogues had the same  $y_{1-4}$  and varying  $b_{1-4}$ .

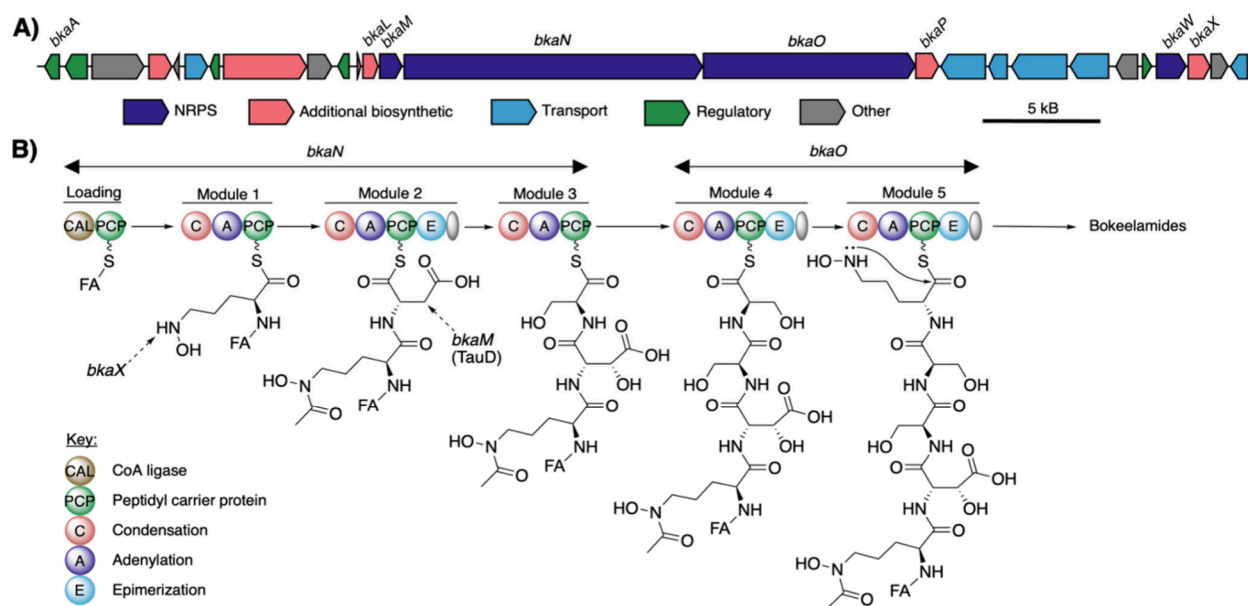


**Figure 3.** (A) Putative BGC responsible for producing bokeelamides and (B) putative enzymatic route to the production of bokeelamides.

fragmentation patterns for the final two nodes, 802 and 830, indicated incorporation of C13:1 and C15:1, respectively, but the position of the unsaturation could not be identified.

Absolute stereochemistry of compounds 1–4 was determined by Marfey's analysis. An aliquot of each compound was hydrolyzed and derivatized with 1-fluoro-2,4-dinitrophenyl-5-L-alanine amide (L-FDAA). A liquid chromatography–mass spectrometry (LCMS) comparison of the derivatized hydrolyzate products to authentic standards revealed the presence of *L*-erythro- $\beta$ OH-Asp (51.8 min), both *L*- and *D*-Ser (51.5 and 52.5 min), and both *L*- and *D*-Orn (83.6 and 78.4 min) (Figures S35–S38 of the Supporting Information). To unequivocally assign the stereoconfiguration of the two Ser and Orn residues, we turned to genomic analysis. *E. khazarica* EM133 genomic DNA was sequenced using the Oxford Nanopore platform, assembled by SeqCenter, and identified by the Type Genome Server (Figure S39 and Table S6 of the Supporting Information). AntiSMASH 7.1.0<sup>14</sup> analysis of the assembled genome identified eight biosynthetic gene clusters (BGCs), with one BGC annotated as a hybrid polyketide synthase (PKS)/nonribosomal peptide synthetase (NRPS) metallophore cluster (Figure 3A). This BGC, named *bka*, contains five NRPS modules with adenylation domains predicted to load the amino acids observed in bokeelamides (Figure 3B). Modules 3 and 4 are predicted to install the Ser residues, while modules 1 and 5 install the modified Orn residues. Excitedly, of these, only modules 4 (Ser<sub>1</sub>) and 5 (Orn<sub>1</sub>) contained epimerization domains, allowing us to assign the absolute stereoconfiguration of compounds 1–9 as *D*-(cyclic-N<sup>5</sup>OH-Orn<sub>1</sub>)-*D*-Ser<sub>1</sub>-*L*-Ser<sub>2</sub>-*L*-(erythro- $\beta$ OH-Asp)-*L*-(AcN<sup>5</sup>OH-Orn<sub>2</sub>)-lipid.

Detailed analysis of the *bka* BGC provided key biochemical and structural information in support of the structure of bokeelamides. The lipid tail is loaded onto the peptidyl carrier protein (PCP) by a CoA ligase (CAL), which is then followed by five NRPS domains that load N<sup>5</sup>OH-Orn<sub>2</sub>, Asp, Ser<sub>2</sub>, Ser<sub>1</sub>, and N<sup>5</sup>OH-Orn<sub>1</sub>. Ornithine 5-monooxygenase, *bkaW*, is predicted to hydroxylate both Orn residues, producing N<sup>5</sup>OH-Orn prior to loading on the adenylation domains.<sup>15</sup> The acylation of Orn<sub>2</sub> is believed to be installed by *bkaX*, a *N*-

acetyltransferase, after Orn<sub>2</sub> has been incorporated into the linear peptide (Table S7 of the Supporting Information). Furthermore, TauD family T $\beta$ H<sub>Asp</sub> aspartyl  $\beta$ -hydroxylase (*bkaM*) has precedent to hydroxylate the  $\beta$  position of Asp, resulting in the observed *R* configuration.<sup>16</sup> The role of the epimerization domain within module 2 is unknown as Marfey's analysis unequivocally assigns  $\beta$ OH-Asp as 2*S*,3*R*-Asp (*erythro*). Previous literature precedence suggests that BGCs containing both TauD and an epimerization domain within the Asp module results in *D*-threo- $\beta$ OH-Asp (2*R*,3*R*-Asp);<sup>16</sup> however, there are exceptions to this finding.<sup>17</sup> Finally, the biosynthesis of bokeelamides is hypothesized to be terminated through intramolecular cyclization of terminal N<sup>5</sup>OH-Orn<sub>1</sub>. However, it is unclear whether this is catalyzed by *bkaL* (NRPS thioesterase) or *bkaP* (an esterase).

Structurally, bokeelamides contain several distinct characteristics of siderophores, including incorporation of both hydroxamates and  $\alpha$ -hydroxycarboxylates, thus indicating that compounds 1–9 are likely functioning as siderophores.<sup>18</sup> The hydroxamate and  $\beta$ OH-Asp moieties are known to bind Fe<sup>3+</sup> and are commonly found in peptidic siderophores, including amphibactins,<sup>19</sup> loihichelins,<sup>20</sup> amychelins,<sup>18</sup> and potashchelins.<sup>21</sup> Many of these siderophores also belong to the large class of amphiphilic lipopeptides, which attach a variety of lipids to a peptidic portion that contains multiple iron-binding ligands.<sup>22,23</sup> The long lipid tail anchors the siderophore to the membrane, keeping it close to the cell membrane. The *bka* BGC further supports that bokeelamides are functioning as siderophores as several genes encode for ferric hydroxamate ABC transporters and TonB-dependent siderophore receptors (*bkaQ-T,Z*; Table S7 of the Supporting Information).<sup>24</sup> Reevaluation of the LCMS chromatograms revealed the presence of both apo- and Fe<sup>3+</sup>-bokeelamides (Figures S40–S43 of the Supporting Information). To further confirm that bokeelamides function as siderophores, Fe<sup>3+</sup>-binding affinities and metal chelation selectivity studies were conducted on both compounds 1 and 2. First, pFe<sup>III</sup> values for compounds 1 and 2 were quantified using an ethylenediaminetetraacetic acid (EDTA) titration assay,<sup>25</sup> which were determined to be 25.9  $\pm$  0.2 and 25.7  $\pm$  0.2, respectively (Figures S44 and S45 of the

Supporting Information). These values are in the range of other amphiphilic lipopeptide siderophores.<sup>18</sup> In addition, both compounds **1** and **2** are capable of chelating Fe<sup>3+</sup> and Ga<sup>3+</sup> but not Zn<sup>2+</sup>, Cu<sup>2+</sup>, or Co<sup>2+</sup> (Figures S46 and S47 of the Supporting Information). When the metals are present in a mixture, there is a 6-fold selectivity for Fe<sup>3+</sup>-bokeelamide versus Ga<sup>3+</sup>-bokeelamide.

Environmental iron is largely insoluble, thereby limiting its bioavailability.<sup>26</sup> Bacterial siderophores are secreted to scavenge Fe<sup>3+</sup>; however, only bacterial species with specific importers can uptake Fe<sup>3+</sup>-bound metabolites.<sup>27</sup> Therefore, siderophores further limit Fe<sup>3+</sup> availability, and by consequence, siderophores have been implicated in shaping host–microbe interactions by inhibiting growth of competing microorganisms.<sup>25,26</sup> Given this precedent, we evaluated purified compounds **1–4** in a range of assays, including antibacterial (e.g., *Staphylococcus aureus* and *Escherichia coli*), antifungal (e.g., *Fusarium keritoplasticum*, *Aspergillus flavus*, and *Candida albicans*), antibiofilm, and red blood cell lysis assays. No activity was observed for any of the compounds at concentrations up to 50 μM (Figures S48–S53 of the Supporting Information). The lack of toxicity toward the various microbial pathogens suggests that compounds **1–4** may not serve a defensive role, but their ability to sequester Fe<sup>3+</sup> could still shape the overall microbial community within the egg masses. Future work will be needed to fully understand the ecological role of bokeelamides within this system.

## ■ ASSOCIATED CONTENT

### Data Availability Statement

The data underlying this study are available in the published article and its Supporting Information and GNPS at <https://gnps.ucsd.edu/ProteoSAFe/status.jsp?task=6d7d6ca7584c41ee800a2b0888d49a52>, MassIVE Repository under accession number MSV000094443 (DOI: 10.25345/C55D8NR8T) at <https://massive.ucsd.edu/ProteoSAFe/dataset.jsp?accession=MSV000094443>, NCBI under accession number JBHEGD010000000 at <https://www.ncbi.nlm.nih.gov/nucleotide/JBHEGD010000000>, and NP-MRD under accession numbers NP0341802 (DOI: 10.57994/3288), NP0341803 (DOI: 10.57994/3289), NP0341804 (DOI: 10.57994/3290), and NP0341805 (DOI: 10.57994/3291) at <https://np-mrd.org/>.

### Supporting Information

The Supporting Information is available free of charge at <https://pubs.acs.org/doi/10.1021/acs.orglett.4c03470>.

NMR and MS data, Marfey's analysis results, genomics data on *E. khazarica* EM133, and bioassay data (PDF)

## ■ AUTHOR INFORMATION

### Corresponding Author

Emily Mevers – Department of Chemistry, Virginia Tech, Blacksburg, Virginia 24061, United States; [orcid.org/0000-0001-7986-5610](https://orcid.org/0000-0001-7986-5610); Email: [emevers@vt.edu](mailto:emevers@vt.edu)

### Authors

Rose Campbell – Department of Chemistry, Virginia Tech, Blacksburg, Virginia 24061, United States; [orcid.org/0009-0009-4100-4845](https://orcid.org/0009-0009-4100-4845)

Lois Kyei – Department of Chemistry, Virginia Tech, Blacksburg, Virginia 24061, United States; [orcid.org/0000-0002-8315-3488](https://orcid.org/0000-0002-8315-3488)

Karla PIEDL – Department of Chemistry, Virginia Tech, Blacksburg, Virginia 24061, United States

Zheyue Zhang – Department of Chemistry, Virginia Tech, Blacksburg, Virginia 24061, United States

Ming Chen – Department of Chemistry, Virginia Tech, Blacksburg, Virginia 24061, United States; [orcid.org/0000-0002-9841-8274](https://orcid.org/0000-0002-9841-8274)

Complete contact information is available at: <https://pubs.acs.org/doi/10.1021/acs.orglett.4c03470>

## Notes

The authors declare no competing financial interest.

## ■ ACKNOWLEDGMENTS

This work was funded by the National Institutes of Health (NIH) [R35 GM146740 (to Emily Mevers) and R35 GM147523 (to Ming Chen)], the Virginia Tech Startup Funds (to Emily Mevers), and the National Science Foundation (NSF) Graduate Research Fellowship Program [DGE2235205 (to Rose Campbell)]. The authors thank the Virginia Tech NMR and Surface Analysis facilities for analytical services and E. Gentry (Department of Chemistry at Virginia Tech) for the use of their Orbitrap mass spectrometer.

## ■ REFERENCES

- Atanasov, A. G.; Zotchev, S. B.; Dirsch, V. M.; Supuran, C. T. Natural Products in Drug Discovery: Advances and Opportunities. *Nat. Rev. Drug Discovery* **2021**, *20* (3), 200–216.
- Newman, D. J.; Cragg, G. M. Natural Products as Sources of New Drugs over the Nearly Four Decades from 01/1981 to 09/2019. *J. Nat. Prod.* **2020**, *83* (3), 770–803.
- Cragg, G. M.; Newman, D. J. Natural Products: A Continuing Source of Novel Drug Leads. *Biochim. Biophys. Acta* **2013**, *1830* (6), 3670–3695.
- Adnani, N.; Rajski, S. R.; Bugni, T. S. Symbiosis-Inspired Approaches to Antibiotic Discovery. *Nat. Prod. Rep.* **2017**, *34* (7), 784–814.
- Van Arnam, E. B.; Currie, C. R.; Clardy, J. Defense Contracts: Molecular Protection in Insect-Microbe Symbioses. *Chem. Soc. Rev.* **2018**, *47* (5), 1638–1651.
- McFall-Ngai, M. J. The Importance of Microbes in Animal Development: Lessons from the Squid-Vibrio Symbiosis. *Annu. Rev. Microbiol.* **2014**, *68* (1), 177–194.
- Flórez, L. V.; Biedermann, P. H. W.; Engl, T.; Kaltenpoth, M. Defensive Symbioses of Animals with Prokaryotic and Eukaryotic Microorganisms. *Nat. Prod. Rep.* **2015**, *32* (7), 904–936.
- Cantley, A. M.; Clardy, J. Animals in a Bacterial World: Opportunities for Chemical Ecology. *Nat. Prod. Rep.* **2015**, *32* (7), 888–892.
- Piedl, K.; Aylward, F. O.; Mevers, E. The Microbiota of Moon Snail Egg Collars Is Shaped by Host-Specific Factors. *Microbiol. Spectrum* **2024**, No. e0180424.
- Kyei, L.; Piedl, K.; Menegatti, C.; Miller, E. M.; Mevers, E. Discovery of Biofilm Inhibitors from the Microbiota of Marine Egg Masses. *J. Nat. Prod.* **2024**, *87* (6), 1635–1642.
- Laatsch, H. *AntiBase 2014: The Natural Compound Identifier*; MSP Kofel: Zollikofen, Switzerland, 2014; [https://www.msp.ch/wp/wp-content/uploads/2014/11/9783527338412\\_Wiley\\_AntiBase\\_2014.pdf](https://www.msp.ch/wp/wp-content/uploads/2014/11/9783527338412_Wiley_AntiBase_2014.pdf) (accessed Feb 5, 2022).
- van Santen, J. A.; Poynton, E. F.; Iskakova, D.; McMann, E.; Alsup, T. A.; Clark, T. N.; Fergusson, C. H.; Fewer, D. P.; Hughes, A.

H.; McCadden, C. A.; Parra, J.; Soldatou, S.; Rudolf, J. D.; Janssen, E. M.-L.; Duncan, K. R.; Linington, R. G. The Natural Products Atlas 2.0: A Database of Microbially-Derived Natural Products. *Nucleic Acids Res.* **2022**, *50* (D1), D1317–D1323.

(13) Dührkop, K.; Fleischauer, M.; Ludwig, M.; Aksenov, A. A.; Melnik, A. V.; Meusel, M.; Dorrestein, P. C.; Rousu, J.; Böcker, S. SIRIUS 4: A Rapid Tool for Turning Tandem Mass Spectra into Metabolite Structure Information. *Nat. Methods* **2019**, *16* (4), 299–302.

(14) Blin, K.; Shaw, S.; Augustijn, H. E.; Reitz, Z. L.; Biermann, F.; Alanjary, M.; Fetter, A.; Terlouw, B. R.; Metcalf, W. W.; Helfrich, E. J. N.; van Wezel, G. P.; Medema, M. H.; Weber, T. AntiSMASH 7.0: New and Improved Predictions for Detection, Regulation, Chemical Structures and Visualisation. *Nucleic Acids Res.* **2023**, *51* (W1), W46–W50.

(15) Bachmann, B. O.; Ravel, J. Chapter 8. Methods for in Silico Prediction of Microbial Polyketide and Nonribosomal Peptide Biosynthetic Pathways from DNA Sequence Data. *Methods Enzymol.* **2009**, *458*, 181–217.

(16) Reitz, Z. L.; Hardy, C. D.; Suk, J.; Bouvet, J.; Butler, A. Genomic Analysis of Siderophore  $\beta$ -Hydroxylases Reveals Divergent Stereocontrol and Expands the Condensation Domain Family. *Proc. Natl. Acad. Sci. U. S. A.* **2019**, *116* (40), 19805–19814.

(17) Baars, O.; Zhang, X.; Gibson, M. I.; Stone, A. T.; Morel, F. M. M.; Seyedsayamdost, M. R. Crochelins: Siderophores with an Unprecedented Iron-Chelating Moiety from the Nitrogen-Fixing Bacterium *Azotobacter chroococcum*. *Angew. Chem., Int. Ed. Engl.* **2018**, *57* (2), 536–541.

(18) Seyedsayamdost, M. R.; Traxler, M. F.; Zheng, S.-L.; Kolter, R.; Clardy, J. Structure and Biosynthesis of Amychelin, an Unusual Mixed-Ligand Siderophore from *Amycolatopsis* sp. AA4. *J. Am. Chem. Soc.* **2011**, *133* (30), 11434–11437.

(19) Martinez, J. S.; Carter-Franklin, J. N.; Mann, E. L.; Martin, J. D.; Haygood, M. G.; Butler, A. Structure and Membrane Affinity of a Suite of Amphiphilic Siderophores Produced by a Marine Bacterium. *Proc. Natl. Acad. Sci. U. S. A.* **2003**, *100* (7), 3754–3759.

(20) Homann, V. V.; Sandy, M.; Tincu, J. A.; Templeton, A. S.; Tebo, B. M.; Butler, A. Loihichelins A–F, a Suite of Amphiphilic Siderophores Produced by the Marine Bacterium *Halomonas* LOB-5. *J. Nat. Prod.* **2009**, *72* (5), 884–888.

(21) Li, Y.; Liu, L.; Zhang, G.; He, N.; Guo, W.; Hong, B.; Xie, Y. Potashchelins, a Suite of Lipid Siderophores Bearing Both *L*-threo and *L*-erythro Beta-Hydroxyaspartic Acids, Acquired from the Potash-Salt-Ore-Derived Extremophile *Halomonas* sp. MG34. *Front. Chem.* **2020**, *8*, 197.

(22) Martinez, J. S.; Butler, A. Marine Amphiphilic Siderophores: Marinobactin Structure, Uptake, and Microbial Partitioning. *J. Inorg. Biochem.* **2007**, *101* (11–12), 1692–1698.

(23) Chen, J.; Guo, Y.; Lu, Y.; Wang, B.; Sun, J.; Zhang, H.; Wang, H. Chemistry and Biology of Siderophores from Marine Microbes. *Mar. Drugs* **2019**, *17* (10), 562.

(24) Galvis, F.; Ageitos, L.; Martínez-Matamoros, D.; Barja, J. L.; Rodríguez, J.; Lemos, M. L.; Jiménez, C.; Balado, M. The Marine Bivalve Mollusc Pathogen *Vibrio neptunius* Produces the Siderophore Amphibactin, Which Is Widespread in Molluscs Microbiota. *Environ. Microbiol.* **2020**, *22* (12), 5467–5482.

(25) Fukuda, T. T. H.; Helfrich, E. J. N.; Mevers, E.; Melo, W. G. P.; Van Arnam, E. B.; Andes, D. R.; Currie, C. R.; Pupo, M. T.; Clardy, J. Specialized Metabolites Reveal Evolutionary History and Geographic Dispersion of a Multilateral Symbiosis. *ACS Cent. Sci.* **2021**, *7* (2), 292–299.

(26) Kramer, J.; Özkaya, Ö.; Kümmerli, R. Bacterial Siderophores in Community and Host Interactions. *Nat. Rev. Microbiol.* **2020**, *18* (3), 152–163.

(27) Hider, R. C.; Kong, X. Chemistry and Biology of Siderophores. *Nat. Prod. Rep.* **2010**, *27* (5), 637–657.